Peer-reviewed version available at *Cells* **2020**, *9*, 1126; doi:10.3390/cells9051126

Article

The cellular protein CAD is recruited into Ebola virus inclusion bodies by the nucleoprotein NP to facilitate genome replication and transcription

Janine Brandt[1], Lisa Wendt[1], Bianca S Bodmer[1], Thomas C Mettenleiter[1], Thomas Hoenen[1]*

[1] Institute of Molecular Virology and Cell Biology, Friedrich-Loeffler-Institut, Greifswald – Insel Riems, Germany

* Correspondence: thomas.hoenen@fli.de

Abstract: Ebola virus (EBOV) is a zoonotic pathogen causing severe hemorrhagic fevers in humans and non-human primates with high case fatality rates. In recent years, the number and extent of outbreaks has increased, highlighting the importance of better understanding the molecular aspects of EBOV infection and host cell interactions to control this virus more efficiently. Many viruses, including EBOV, have been shown to recruit host proteins for different viral processes. Based on a genome-wide siRNA screen, we recently identified the cellular host factor carbamoyl-phosphate synthetase 2, aspartate transcarbamylase, and dihydroorotase (CAD) to be involved in EBOV RNA synthesis. However, mechanistic details of how this host factor plays a role in the EBOV life cycle remain elusive. In this study, we analyzed the functional and molecular interactions between EBOV and CAD. To this end, we used siRNA knockdowns in combination with various reverse-genetics based lifecycle-modelling systems and additionally performed co-immunoprecipitation and co-immunofluorescence assays to investigate the influence of CAD on individual aspects of the EBOV life cycle and to characterize the interactions of CAD with viral proteins. Following this approach, we could demonstrate that CAD directly interacts with the EBOV nucleoprotein NP, and that NP is sufficient to recruit CAD into inclusion bodies dependent on the GLN-domain of CAD. Further, siRNA knockdown experiments indicated that CAD is important for both viral genome replication and transcription, while substrate rescue experiments showed that the function of CAD in pyrimidine synthesis is indeed required for those processes. Together this suggests that NP recruits CAD into inclusion bodies via its GLN domain in order to provide pyrimidines for EBOV genome replication and transcription. These results define a novel mechanism by which EBOV hijacks host cell pathways in order to facilitate genome replication and transcription, and provide further basis for the development of host directed broad spectrum antivirals.

Keywords: Ebola virus; filovirus; inclusion bodies; CAD; pyrimidine synthesis

1. Introduction

Ebola virus (EBOV) is a zoonotic pathogen belonging to the genus *Ebolavirus* within the order *Filoviridae*, and the causative agent of severe hemorrhagic fevers in humans and non-human primates with high case fatality rates [1,2]. Increasing numbers of EBOV outbreaks in Africa highlight the importance to better understand the molecular mechanisms of the EBOV life cycle and virus-host cell interactions in order to develop new countermeasures against this virus. EBOV possesses a non-segmented, single-stranded RNA genome of negative polarity that together with the ribonucleoprotein (RNP) complex proteins forms a helical nucleocapsid in the center of virions. During assembly of the nucleocapsid, the RNA genome is tightly coated with viral nucleoprotein (NP), which protects the genome from degradation and recognition by the cellular immune response [3]. During EBOV infection, NP-associated RNA genomes serve as templates for mRNA transcription

Peer-reviewed version available at Cells 2020, 9, 1126; doi:10.3390/cells9051126

and genome replication [4]. For viral replication, NP interacts with the polymerase cofactor VP35, which acts as a linker between NP and L [5]. NP, VP35, and L are sufficient to facilitate EBOV genome replication, while for viral transcription the transcriptional activator VP30 is additionally required [6,7]. EBOV replication and transcription takes place in cytoplasmic inclusion bodies, which represent a characteristic feature of EBOV infections in cells [8,9]. Their formation can be driven by the single expression of NP [5,10,11]. However, due to the limited number of viral genes, successful genome replication and transcription is highly dependent on host cell factors, which play an important role during the EBOV life cycle. For instance, the host factor STAU-1 has been shown to interact with multiple EBOV RNP components, and to redistribute into NP-induced or virus-induced inclusion bodies, suggesting that STAU-1 plays a crucial role during viral RNA-synthesis by facilitating the interaction between the viral genome and RNP proteins [12]. EBOV has also been shown to recruit SMYD3 into inclusion bodies, which increases NP-VP30 interaction and enhances mRNA transcription [13]. Similarly, RBB6 was identified to influence EBOV replication by disrupting the interaction between NP and VP30 [14]. Importin-α7 was described as required for the efficient formation of inclusion bodies [15]. Furthermore, several cellular kinases and phosphatases are known to localize into inclusion bodies for supporting EBOV replication and transcription [16-18]. Finally, we could previously show that EBOV NP recruits the nuclear RNA export factor 1 (NXF1) into inclusion bodies to facilitate viral mRNA export to the cytoplasm [19]. Despite this recent progress in our understanding of the interplay between host factors and EBOV, there remains a considerable need to identify and more importantly to characterize further host factors required for EBOV replication to identify novel targets for antiviral drug development.

We previously performed a genome-wide siRNA screen using a minigenome system to identify potential host-directed targets [20]. In this system a minigenome, i.e. a truncated version of the EBOV genome lacking all viral open reading frames and consisting of a reporter gene (e.g., luciferase or green fluorescent protein) flanked by the viral non-coding terminal leader and trailer regions, is expressed from a plasmid in mammalian cells together with the plasmids encoding the viral RNP proteins [6]. For initial transcription of the minigenome RNAs from the minigenome-encoding plasmids most existing EBOV minigenome systems use a T7 RNA polymerase (T7) promoter, and therefore require expression of T7 polymerase, which is usually provided via a T7-expressing plasmid that is cotransfected with the plasmids encoding for the RNP proteins [6,21]. However, recently an EBOV minigenome system using the cellular RNA polymerase II (Pol-II) as accessory polymerase for initial minigenome RNA transcription has also been established, and shown to be more efficient at least in some cell types [22]. After initial transcription and encapsidation by RNP proteins minigenome RNAs are recognized as authentic templates by the viral polymerase due to their leader and trailer regions, and are replicated and transcribed into mRNAs, which results in the expression of the reporter protein. Thus, minigenome assays allow us to study viral genome replication and transcription as well as viral protein expression outside of maximum containment laboratories, simplifying the identification of host factors involved in these processes. By using this system, we recently identified the trifunctional protein carbamoyl-phosphate synthetase 2, aspartate transcarbamylase, and dihydroorotase (CAD) to be important for the EBOV life cycle [20].

CAD is an important component of the pyrimidine pathway that catalyzes the first three steps during the *de novo* biosynthesis of pyrimidine nucleotides, and consists of four distinct, enzymatic domains [23-25]. The first domain, glutaminase (GLN), initiates the pathway by catalyzing the hydrolysis of glutamine. This is followed by the synthesis of carbamoyl phosphate facilitated by the carbamoyl-phosphate synthetase (CPS). Carbamoyl phosphate is in turn the substrate for the aspartate transcarbamylase (ATC), which catalyzes the reaction of aspartate with carbamoyl phosphate to carbamoyl aspartate [26,27]. Finally, carbamoyl aspartate is converted to dihydroorotate by dihydroorotase (DHO) [28]. In response to cell growth and proliferation CAD activity is upregulated by phosphorylation through MAP kinases at position Thr-456, while in resting cells Thr-456 is dephosphorylated [29]. Furthermore, CAD is known to primarily localize in the cytoplasm of resting cells, but in response to cell growth and Thr-456 phosphorylation a small fraction is translocated into nuclear compartments, suggesting a cellular function of CAD in the nucleus

Peer-reviewed version available at Cells 2020, 9, 1126; doi:10.3390/cells9051126

[30,31]. However, little is known about the role of CAD during virus infection, and particularly the role of CAD for the EBOV life cycle still needed to be further analyzed. Therefore, we wanted to characterize the interaction of CAD with EBOV on a biochemical and functional level. Based on our results we suggest that CAD is important for both genome replication and transcription due to its function in pyrimidine synthesis, and that it is recruited into NP-induced and virus-induced inclusion bodies to facilitate the *de novo* biosynthesis of pyrimidine nucleotides.

2. Materials and Methods

2.1. Cell lines

Human embryonic kidney cells (HEK 293T, Collection of Cell Lines in Veterinary Medicine CCLV-RIE 1018) and human hepatocellular carcinoma cells (Huh7, kindly provided by Stephan Becker, Philipps University Marburg) were cultured in Dulbecco's modified Eagle's medium (DMEM; ThermoFisher Scientific) supplemented with 10 % fetal calf serum (FCS), 100 U/ml penicillin, 100 µg/ml streptomycin (PS; ThermoFisher Scientific) and 1x GlutaMAX (ThermoFisher Scientific). All cells were incubated at 37 °C and 5 % CO_2.

2.2. Plasmids and cloning

Minigenome assay components, including expression plasmids coding for the EBOV RNP proteins, the T7 polymerase, firefly luciferase, and the classical T7-driven monocistronic minigenome (pT7-1cis-EBOV-vRNA-nLuc) have been previously described [20,32]. A NanoLuc luciferase-expressing T7-driven replication-deficient minigenome was cloned from a classical minigenome expressing NanoLuc luciferase as reporter by deletion of 55 nucleotides (nt) in the antigenomic replication promoter as previously described [32]. Based on this, a Pol-II-driven replication-deficient minigenome was generated by PCR to amplify a linear version of the replication-deficient minigenome flanked by hammerhead and Hepatitis Delta Virus ribozymes using the primers #4571 (5'-AGC TTA CGT GAC TAC TTC CTT CGG ATG CCC AGG TCG GAC CGC G-3') and #4572 (5'-GAC CGG TAG AAA ACT GAT GAG TCC GTG AGG ACG AAA CGG AGT CTA GAC TCC GTC TTT TCC AGG AAT CCT TTT TGC AAC GTT TAT TCT G-3'). The linearized construct was subsequently inserted into pCAGGS. The CAD gene was cloned from 293T cells into pCAGGS, and deletion mutants and domains of CAD were then generated using PCR-based approaches. All constructs were first cloned into pCAGGS, followed by subcloning into a pCAGGS plasmid encoding an N-terminal flag/HA-tag (DYKDDDDKLDGGYPYDVPDYA) immediately upstream of a BsmBI cloning site, allowing a seamless insertion of the open reading frame of interest. The expression plasmid for N-terminally myc-tagged VP35 was constructed by cloning a myc-tag (EQKLISEEDL) immediately before the VP35 ORF. Detailed cloning strategies are available on request.

2.3. Antibodies

The anti-flag (clone M2) antibody used for immunofluorescence analyses (IFA), coIP, and Western Blot analyses was purchased from Sigma-Aldrich [F1804], and the anti-c-myc antibody used for IFA analysis was obtained from ThermoFisher Scientific [A-21281]. Primary antibodies against NP (rabbit anti-EBOV NP polyclonal antibody), GAPDH (mouse anti-GAPDH clone 0411), and CAD (rabbit anti-CAD clone EP710Y) were ordered from IBT Bioservices (anti-NP [0301-012]), Santa Cruz (anti-GAPDH [sc47724]), or Abcam (anti-CAD [ab40800]). Secondary antibodies used for IFA analysis against mouse (Alexa Fluor-488 anti-mouse [A-11029]), rabbit (Alexa Fluor-568 anti-rabbit [A-11036]), and chicken (Alexa Fluor-647 anti-chicken [A-21449]) were obtained from ThermoFisher Scientific. For Western Blot, secondary antibodies against mouse (IRDye 680RD anti-mouse [926-68070]) and rabbit (IRDye 800CW anti-rabbit [926-68071]) were purchased from Li-COR, while anti-mouse IgG (kappa light chain)-Alexa Fluor 680 [115-625-174] used for co-IP analyses was ordered from Dianova.

2.4. Viruses

Peer-reviewed version available at Cells 2020, 9, 1126; doi:10.3390/cells9051126

Zaire ebolavirus rec/COD/1976/Mayinga-rgEBOV (GenBank accession number KF827427.1), which is identical in sequence to the EBOV Mayinga isolate with the exception of four silent mutations as genetic markers [33], was used for all infection experiments. rgEBOV was propagated in VeroE6 cells and virus titers were determined by 50 % tissue culture infectious dose (TCID50) assay. All work with infectious virus was performed under BSL-4 conditions at the Friedrich-Loeffler-Institut (Federal research institute of animal health, Greifswald Insel-Riems, Germany) following approved standard operating procedures.

2.5. Chemical compounds

100 mM uridine or cytidine (both Sigma-Aldrich) stock solutions were prepared in DMSO and further diluted in the appropriate cell culture medium. Diluted pyrimidines or DMSO corresponding to 1 % of the supernatant volume in 12-well plates was added to the cells at the time of transfection, and after medium changes. All concentrations indicated in the figures are final concentrations.

2.6. siRNA knockdown with EBOV minigenomes and pyrimidine complementation

For siRNA knockdown of endogenous CAD, 293T cells were reverse transfected with 12 pmol pre-designed silencer select siRNAs (CAD-siRNA#1: s2320 [5′-GAG GGU CUC UUC UUA AGU A-3′]; CAD-siRNA#2: 117891 [5′-GCU AGC UGA GAA AAA CUU U-3′]; Negative Control siRNA#2; all ThermoFisher Scientific) or an self-designed EBOV-anti-L siRNA [5′-UUU AUA UAC AGC UUC GUA CUU-3′] ordered from Eurofins Genomics. Transfection was performed in 12-well plates using Lipofectamine RNAiMax (ThermoFisher Scientific) following the manufacturer's instructions. 48 hours post siRNA transfection cells were transfected using Transit-LT1 (Mirus Bio LLC) with all minigenome assay components, i.e. pCAGGS-based expression plasmids for NP (62.5 ng), VP35 (62.5 ng), VP30 (37.5 ng), L (500 ng), codon-optimized T7-polymerase (125 ng), firefly luciferase (as control, 125 ng), and the T7-driven monocistronic minigenome (pT7-EBOV-1cis-vRNA-nLuc; 125 ng). For analyses of vRNA and mRNA levels the control firefly luciferase was replaced by GFP (200 ng), and for the replication-deficient minigenome assay a Pol-II-driven replication-deficient minigenome (pCAGGS-EBOV-1cis-vRNA-nLuc-RdM) was used. Transfections were performed using Transit LT1 as previously described [32]. All samples were harvested 48 hours post transfection for either determination of reporter activity or RNA isolation (see below). For measuring the luciferase activity, cells were lysed for 10 min in 1x Lysis Juice (PJK) at room temperature and lysates were cleared from cell debris by centrifugation for 3 min at 10,000 x g. Then, 40 µl of cleared lysate was added to either 40 µl of Beetle Juice (PJK) or NanoGlo Luciferase Assay Reagent (Promega) in opaque 96-well plates, and luminescence was measured using a Glomax Multi (Promega) microplate reader. NanoLuc luciferase activities were normalized to firefly luciferase activities.

2.7. RNA isolation and RT-qPCR

RNA isolation from minigenome cell lysates was performed following the manufacturer's instruction using the NucleoSpin RNA kit (Machery-Nagel). After RNA purification, all samples were treated with DNase (TURBO DNA-free kit; ThermoFisher Scientific) following the manufacturer's instructions to avoid plasmid contamination. For cDNA generation, RNA samples were incubated with oligo(dT)-primers for mRNA quantification, or strand-specific primers (5′-AGT GTG AGC TTC TAA AGC AAC C-3′) for vRNA quantification, using the RevertAid Reverse Transcriptase (ThermoFisher Scientific) following the manufacturer's instructions. The subsequent qPCR was performed using the PowerUp SYBR Green Master Mix (ThermoFisher Scientific) with 1 µl of cDNA and primers targeting either the reporter gene (5′-TTC AGA ATC TCG GG GTG TCC-3′, 5′-CGT AAC CCC GTC GAT TAC CA-3′), or GFP as control (5′-CTT GTA CAG CTC GTC CAT GC-3′, 5′-CGA CAA CCA CTA CCT GAG CAC-3′). Values for vRNA and mRNA levels were normalized to control GFP mRNA levels.

2.8. Immunofluorescence analysis

Peer-reviewed version available at Cells 2020, 9, 1126; doi:10.3390/cells9051126

Huh7 cells were seeded on coverslips in 12-well plates and transfected 24 hours later with 500 ng pCAGGS-EBOV-NP and 500 ng pCAGGS-flag-HA-CAD (or CAD mutants), and in selected experiments additionally with 500 ng pCAGGS-myc-VP35 as indicated. For a mock control, cells were transfected with pCAGGS. Transfection was performed using polyethylenimine (Sigma-Aldrich) following the manufacturer's instructions. 48 h post transfection, cells were fixed using 4 % paraformaldehyde (Roth) in DMEM for 20 min and then treated with 1 M glycin (in phosphate-buffered saline^{++} (PBS with 0.9M Ca^{2+} and 0.5M Mg^{2+})) for 10 min. Then, cells were permeabilized with 0.1 % Triton X-100 in PBS for another 10 min and incubated with 10 % fetal calf serum (FCS) in PBS for 45 min. Primary antibodies (rabbit anti-EBOV-NP 1:500; mouse anti-flag 1:2,500; chicken anti-myc 1:1,200) were diluted in PBS with 10 % FCS and cells were incubated for 1 hour at room temperature with the prepared antibody solutions. Secondary antibodies (Alexa Fluor-488 anti-mouse 1:1,200; Alexa Fluor-568 anti-rabbit 1:500; Alexa Fluor-647 anti-chicken 1:1,200) were prepared as described for the primary antibodies. After 45 min staining, cells were washed with PBS and water before mounting with ProLong Diamond Antifade mountant with DAPI (ThermoFisher Scientific). Slides were analyzed by confocal laser scanning microscopy using a Leica SP5.

2.9. Infection of transfected Huh7 cells

To investigate the localization of CAD during EBOV infection, Huh7 cells were seeded in 8-well chambered slides (ibidi) and transfected as described above (Immunofluorescence analysis) with 500 ng pCAGGS-flag/HA-CAD. At 48 hours post transfection, the transfected cells were infected with EBOV at an MOI of 1, and samples were fixed 16 hours post infection in 10 % formalin twice over night prior to removal from the BSL4 facility and immunofluorescence analysis.

2.10. Co-immunoprecipitation of viral proteins

Co-immunoprecipitation assays (coIPs) were performed as previously described [19]. Briefly, 293T cells were seeded in 6-well plates and transfected with expression plasmids encoding for flag/HA-tagged CAD and EBOV-NP using Transit LT-1 (Mirus Bio LLC) following the manufacturer's instructions. Medium was exchanged after 24 hours and cells were harvested 48 hours post transfection. For coIP, cells were lysed in 1 ml coIP lysis buffer (1 % NP-40; 50 mM Tris pH 7.4; 167 mM NaCl in Millipore water) with protease inhibitor (cOmplete; Roche). To investigate a possible RNA-dependency of the interaction between CAD and NP, 100 µg/ml RNase A (Machery-Nagel) was added to the samples. Subsequently, samples were incubated rotating at 15 RPM for 2 hours at 4 °C. Then, 150 µl of the cleared lysates were taken as input control (representing a sixth of the complete pre-immune lysate and 20 % of the sample used for IP), and subjected to acetone precipitation. The remaining 750 µl of the cell lysate was mixed with the prepared bead-antibody solution (Dynabeads Protein G, ThermoFisher Scientific; 1 µl anti-flag M2 antibody per 10 µl beads). IP was performed for 10 min, as recommended by the manufacturer, at room temperature and rotating at 15 RPM. Then samples were transferred to new tubes and boiled for 10 min at 99 °C. Input and coIP samples were analyzed by SDS-PAGE and Western Blot.

2.11. Western Blot

For validation of CAD knockdown efficiency and analyses of coIP input and lysates, samples were subjected to SDS-PAGE and Western blotting as previously described [34]. Flag-tagged CAD was detected using a monoclonal anti-flag antibody (1:2,000), while NP, CAD-WT, and GAPDH were detected using anti-NP (1:1000), anti-CAD (1:250), and anti-GAPDH (1:1,000) antibodies. As secondary antibodies, 680RD-coupled goat-anti-mouse, goat-anti-mouse-Alexa Fluor-680, and 800CW-coupled goat-anti-rabbit (1:14,000) were used. Fluorescent signals were detected and quantified using an Odyssey CLx infrared imaging system (Li-Cor Biosciences). For knockdown quantification, CAD signals were normalized to GAPDH signals.

2.12. Statistical analyses

Peer-reviewed version available at Cells 2020, 9, 1126; doi:10.3390/cells9051126

One-way ANOVA with Dunett's multiple comparisons test was performed using the GraphPad Prism 8 software.

3. Results

3.1. CAD knockdown affects both EBOV genome replication and transcription

Using a genome-wide siRNA screen, we previously identified CAD to be important for EBOV RNA synthesis and/or viral protein expression [20]. However, since only the effect of CAD knockdown on the sum of these processes had been tested, we now analyzed the role of CAD on individual aspects of the EBOV life cycle. As a first step, we assessed the efficiency of knockdown of endogenous CAD using two different siRNAs via quantitative Western Blot, which revealed a 60 % to 80 % reduction in endogenous CAD expression levels for the two siRNAs (Figure 1A and B).

Based on this, we next performed a classical minigenome assay in connection with an siRNA knockdown of CAD. As previously shown, knockdown of CAD led to a 40 to 53-fold reduction in reporter activity, verifying an influence of CAD on EBOV viral RNA synthesis and protein expression (Figure 1C) [20]. In order to identify whether CAD knockdown affects transcription and/or protein expression independent of replication, we next used a replication-deficient minigenome system [32]. In contrast to a replication-competent minigenome, the replication-deficient minigenome lacks 55 nt in the antigenomic replication promoter, leading to a block of minigenome vRNA replication, while minigenome transcription is still taking place [32]. However, when using this system, which is based on T7-driven initial transcription of minigenomes, we observed a very low dynamic range between our controls, which made it difficult to evaluate a possible influence of CAD knockdown (Figure S1). Therefore, in order to increase the dynamic range of this system, we generated a Pol-II-driven replication-deficient minigenome that resulted in a ~ 10 fold higher dynamic range (Figure S1). Using this system, CAD knockdown resulted in a clear reduction in reporter activity, indicating that CAD is, independent of viral genome replication, important for EBOV transcription and/or protein expression (Figure 1D).

To further dissect the influences of CAD on viral genome replication, mRNA transcription, and later steps of viral protein expression, we performed classical minigenome assays in context of an siRNA knockdown of CAD, and measured vRNA and mRNA levels in cell lysates via RT-qPCR. CAD siRNA-treated cells showed a strong reduction in both vRNA and mRNA levels in comparison to the control cells, demonstrating that CAD is important for both EBOV transcription and viral genome replication (Figure 1E and F).

Peer-reviewed version available at Cells 2020, 9, 1126; doi:10.3390/cells9051126

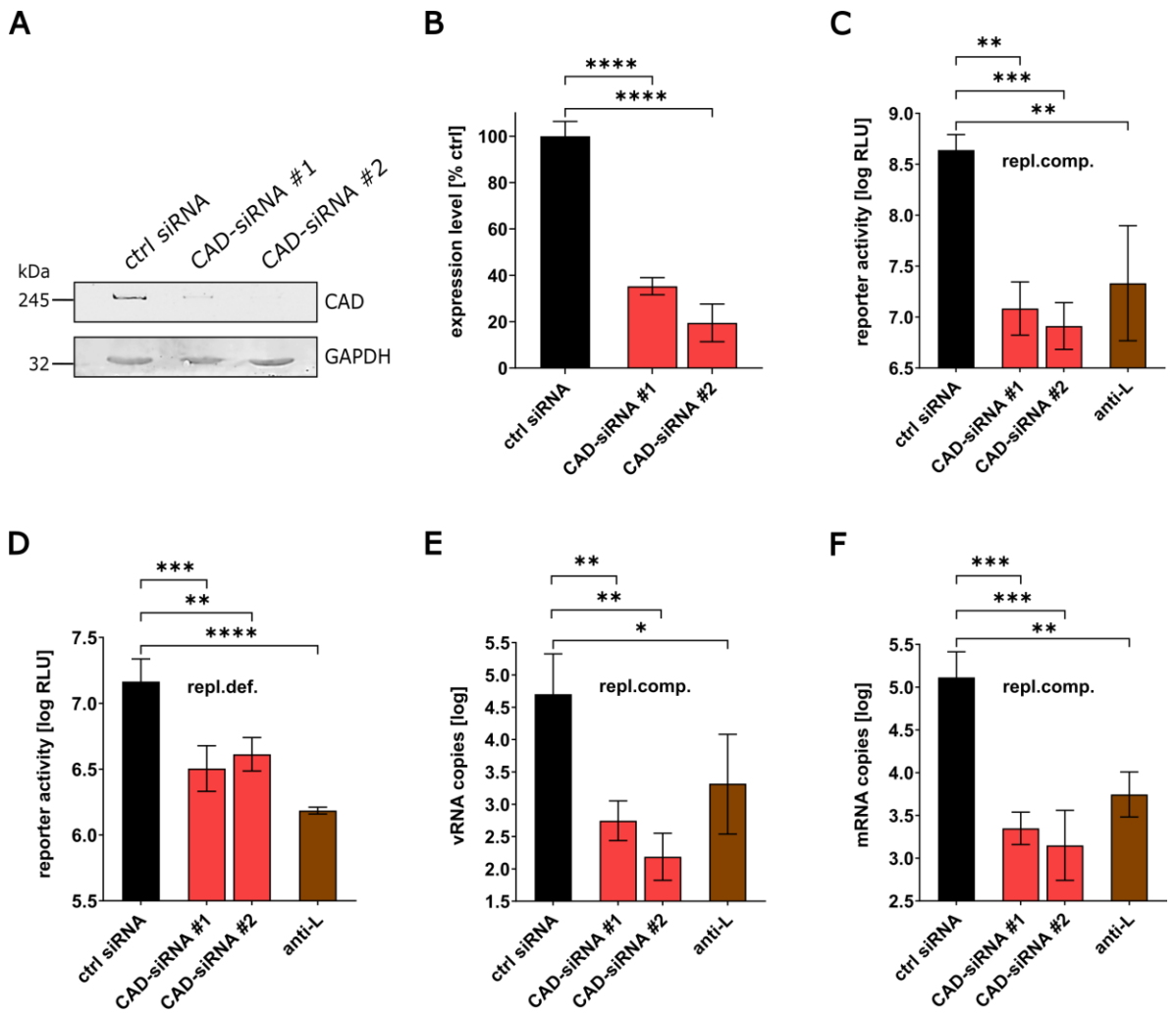

Figure 1. Influence of CAD knockdown on Ebola virus life cycle. (A) Analysis of CAD knockdown. 293T cells were transfected with siRNAs targeting CAD (CAD-siRNA) or a negative control (ctrl siRNA). Cells were harvested 48 hours post transfection and lysates were subjected to SDS-PAGE and Western Blot. **(B)** Quantification of CAD knockdown. Western Blot signals for CAD knockdown (as shown in Figure 1A) were measured and normalized to GAPDH signals. The negative control (ctrl siRNA) was set to 100 % and the efficiency of CAD knockdown was calculated. **(C)** Influence of CAD knockdown on EBOV RNA synthesis. 293T cells were transfected with siRNAs targeting either CAD (CAD-siRNA), EBOV-L (anti-L), or a negative control (ctrl siRNA). 48 hours post transfection, cells were transfected with all components required for a replication-competent minigenome (repl.comp.). Another 48 hours later, cells were harvested and reporter activity was measured. **(D)** Analysis of CAD knockdown on EBOV transcription and gene expression. 293T cells were transfected with siRNAs targeting either CAD (CAD-siRNA), EBOV-L (anti-L), or a negative control (ctrl siRNA). 48 hours post transfection, cells were transfected with all components required for a replication-deficient minigenome (repl.def.). Another 48 hours later, cells were harvested and reporter activity was measured. **(E)** Impact of CAD knockdown on EBOV replication. Cells were treated as described in 1C. After cell harvest, RNA was extracted from cell lysates and RT-qPCR for vRNA was performed. **(F)** Influence of CAD knockdown on EBOV mRNA levels. Cells were treated as described in 1C. After cell harvest, RNA was extracted from cell lysates and RT-qPCR for mRNA was performed. Means and standard deviations of 3 independent experiments are shown for each panel. Asterisks indicate p values from one-way ANOVA (*: $p \leq 0.05$; **: $p \leq 0.01$; ***: $p \leq 0.001$; ****: $p \leq 0.0001$; ns: $p > 0.05$).

3.2. The effect of CAD knockdown can be compensated by exogenous pyrimidines

Peer-reviewed version available at Cells 2020, 9, 1126; doi:10.3390/cells9051126

As CAD is an important component for pyrimidine synthesis [23], we wanted to investigate the effect of providing exogenous pyrimidines on EBOV transcription and replication during siRNA knockdown of CAD. To this end, we performed an siRNA-mediated knockdown of CAD with EBOV minigenomes and treated cells with 1 mM of either uridine or cytidine. Complementation of uridine resulted in reporter activities similar to the positive controls, indicating that the effect of CAD knockdown on EBOV genome replication and transcription is due to a lack of pyrimidines (Figure 2). When providing cytidine, a similar rescue effect was seen, albeit less pronounced, possibly because cytidine is not metabolized into uridine, whereas exogenous uridine can be metabolized into cytidine during the natural pyrimidine synthesis.

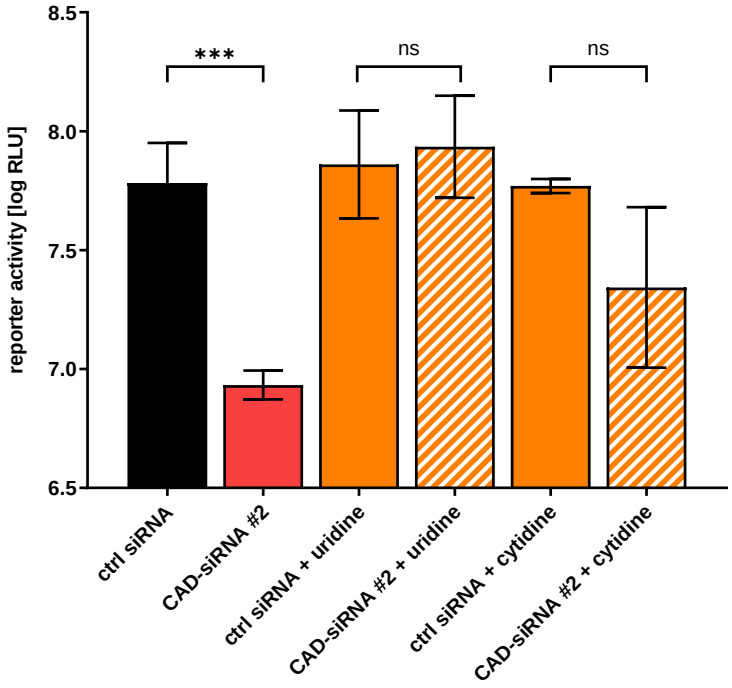

Figure 2. Supplementation of pyrimidines compensates the effect of CAD knockdown. 293T cells were transfected with siRNAs targeting CAD (CAD-siRNA) or a negative control (ctrl siRNA). 48 hours post transfection cells were transfected with all components required for a replication-competent minigenome and treated with 1 mM pyrimidines, either uridine or cytidine. Another 48 hours later, cells were harvested and reporter activity was measured. Means and standard deviations of 3 independent experiments are shown. Asterisks indicate p values from one-way ANOVA (***: $0.0001 < p \leq 0.001$; ns: $p > 0.05$).

3.3. CAD colocalizes with NP-induced inclusion bodies

Similar to other negative-sense RNA viruses, EBOV and in particular its nucleoprotein NP is known to induce the formation of cytoplasmic inclusion bodies that are sites of viral genome replication and transcription [8,9]. Since we have shown that CAD is important for EBOV replication and transcription, we wanted to investigate whether the presence of inclusion bodies has an influence on the intracellular distribution of CAD, and in particular whether recruitment of CAD into NP-induced inclusion bodies can be detected. As previously reported, expression of only NP resulted in the formation of inclusion bodies predominantly in the perinuclear region [5,10,11], while sole expression of CAD led to an even distribution throughout the cytoplasm, with small amounts of CAD present in the nucleus [30] (Figure 3A). During co-expression of NP and CAD we observed relocalization of CAD into NP-induced inclusion bodies. When we additionally coexpressed VP35, which is involved in nucleocapsid formation during EBOV infection together with NP [35], we observed a similar phenotype (Figure 3B). To confirm these results, we also performed experiments with infectious EBOV and stained the samples for NP, as an inclusion body marker, and CAD (Figure

Peer-reviewed version available at Cells 2020, 9, 1126; doi:10.3390/cells9051126

4). Colocalization of CAD and inclusion bodies was still detectable, albeit not as apparent as under conditions of recombinant overexpression of NP and VP35. Taken together these results suggest that CAD is recruited into viral inclusion bodies to provide sufficient amounts of pyrimidines for EBOV genome replication and transcription.

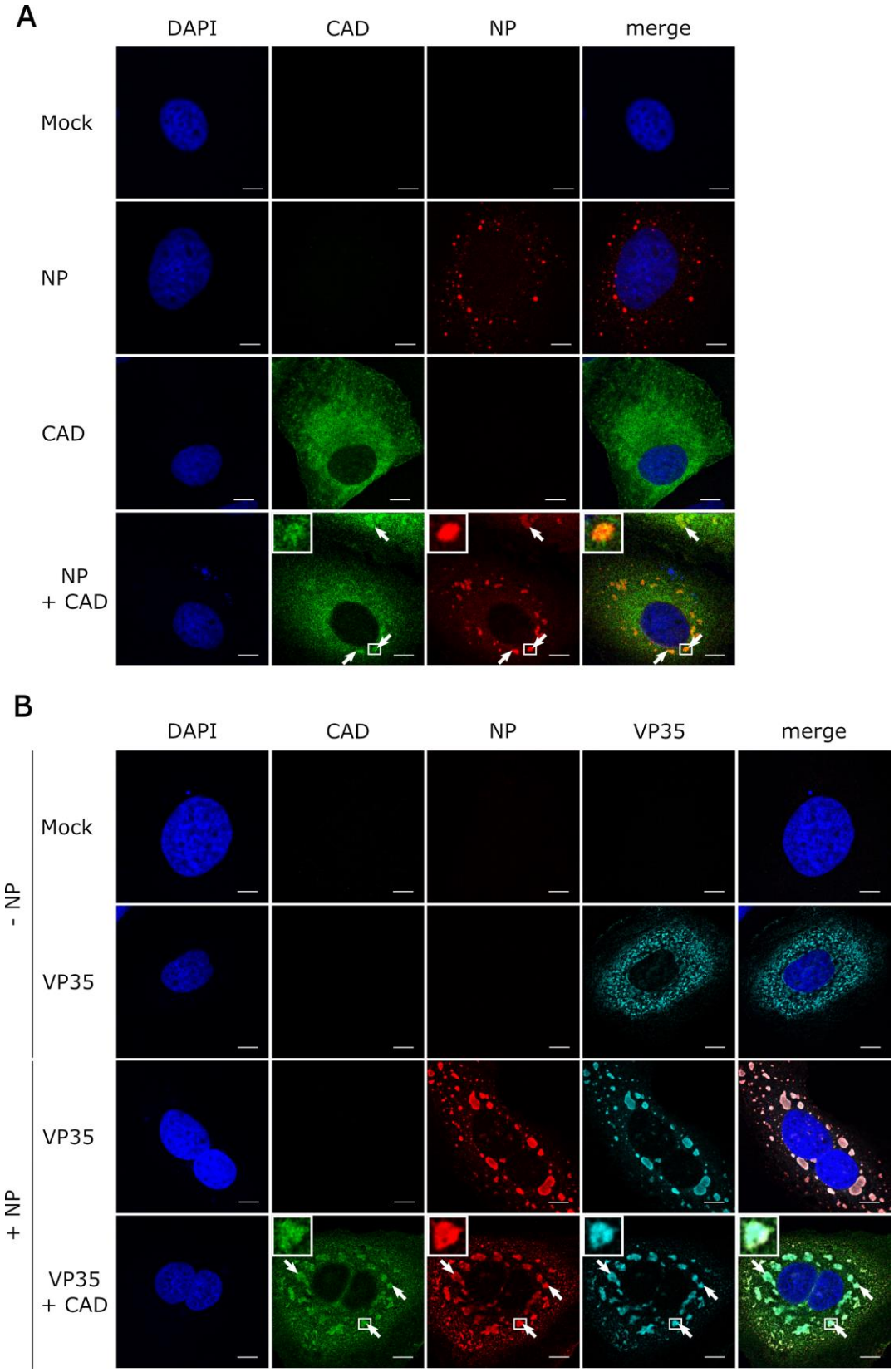

Figure 3: Recruitment of CAD into NP-induced inclusion bodies. (A) Colocalization between CAD and NP-induced inclusion bodies. Huh7 cells were transfected with plasmids encoding for flag/HA-

Peer-reviewed version available at Cells 2020, 9, 1126; doi:10.3390/cells9051126

CAD and EBOV-NP as indicated. 48 hours post transfection cells were fixed with 4 % PFA and permeabilized with 0.1 % Triton X-100. Flag-tagged CAD (shown in green) was detected using an anti-flag antibody and NP (shown in red) was stained with anti-EBOV NP antibodies. **(B)** Recruitment of CAD into inclusion bodies occurs in presence of VP35. Huh7 cells were transfected with plasmids encoding for flag/HA-CAD, EBOV-NP, and myc-EBOV-VP35 as indicated. 48 hours post transfection cells were fixed with 4 % PFA and permeabilized with 0.1 % Triton X-100. Flag-tagged CAD (shown in green) was detected using an anti-flag antibody, NP (shown in red) was stained with anti-EBOV NP antibodies, and myc-tagged VP35 (shown in turquoise) with an anti-myc antibody. Nuclei were stained with DAPI (shown in blue), and cells were visualized by confocal laser scanning microscopy. Scale bars indicate 10 µm. Arrows point out colocalization, and insets show magnifications of indicated areas.

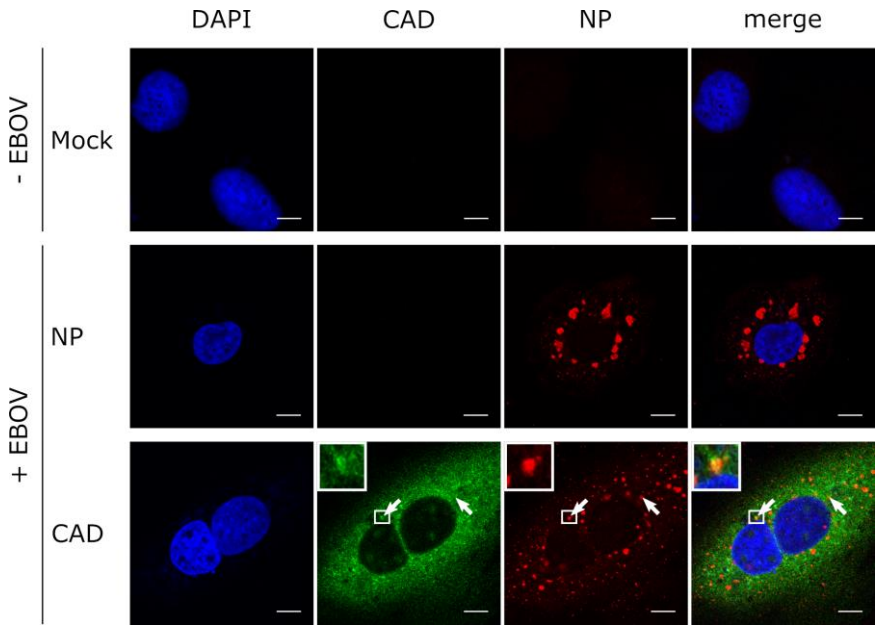

Figure 4. CAD localizes into EBOV inclusion bodies. Huh7 cells were transfected with plasmids encoding for flag/HA-CAD. 48 hours post transfection cells were infected with rgEBOV at an MOI of 1. After incubation of 16 hours, cells were fixed with 10 % formalin and permeabilized with Triton X-100. CAD (shown in green) was detected with an anti-flag antibody and NP (shown in red) with an anti-NP antibody. Nuclei were stained with DAPI (shown in blue), and cells were visualized by confocal laser scanning microscopy. Scale bars indicate 10 µm. Arrows point out colocalization, and insets show magnifications of indicated areas.

3.4. The GLN-domain of CAD is required for accumulation in inclusion bodies

To assess the contribution of individual domains of CAD on the recruitment into NP-induced inclusion bodies, we focused on the GLN and the CPS domain. When we expressed deletion mutants of these domains, they showed a similar intracellular distribution compared to wild type CAD when expressed alone in the cells. During co-expression of NP and CAD-ΔCPS, we observed recruitment of this mutant into NP-driven inclusion bodies, indicating that the CPS domain of CAD is not required for accumulation in inclusion bodies (Figure 5). In stark contrast, when NP was expressed together with CAD-ΔGLN, colocalization with inclusion bodies was abolished, suggesting that the GLN domain is required for recruitment and accumulation into NP-induced inclusion bodies.

Peer-reviewed version available at Cells 2020, 9, 1126; doi:10.3390/cells9051126

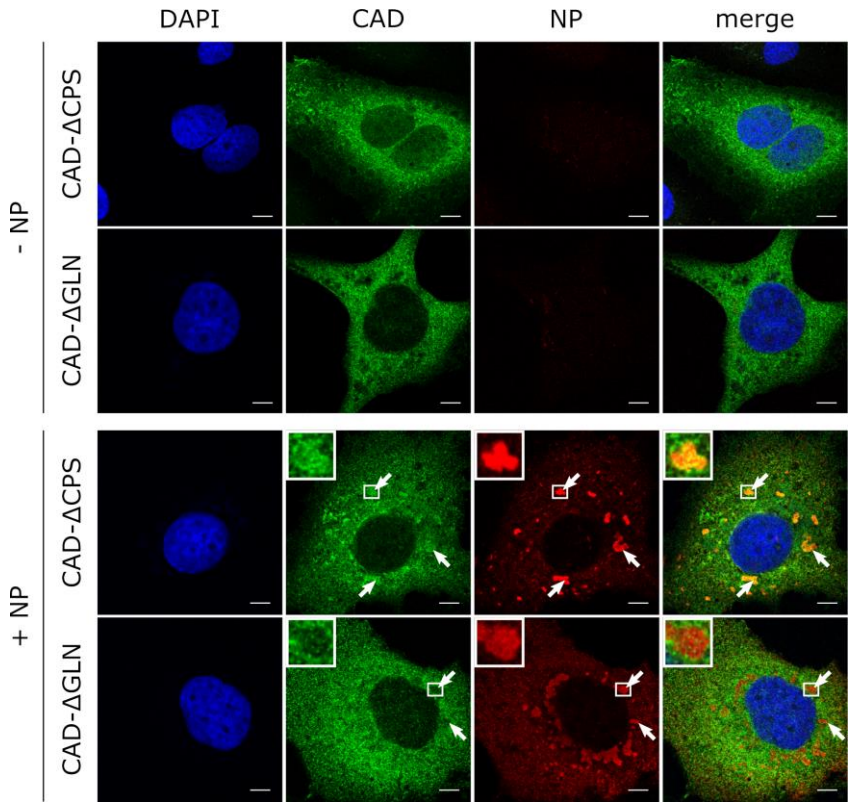

Figure 5. Recruitment of CAD deletions-mutants into inclusion bodies. Huh7 cells containing overexpressed flag/HA CAD-ΔGLN, flag/HA CAD-ΔCPS and EBOV-NP as indicated were fixed with 4 % PFA and permeabilized with 0.1 % Triton X-100 48 hours post transfection. Flag-tagged CAD (shown in green) was detected using an anti-flag antibody and NP (shown in red) was stained with EBOV anti-NP antibodies. Nuclei were stained with DAPI (shown in blue), and cells were visualized by confocal laser scanning microscopy. Scale bars indicate 10 µm. Arrows point out inclusion bodies, and insets show magnifications of indicated areas.

3.5. CAD interacts with NP in an RNA-independent manner

As NP recruits CAD into EBOV inclusion bodies, we next assessed whether CAD interacts with NP. To this end, we performed coIP assays using flag-CAD expressed in the presence of NP by precipitating CAD with an anti-flag antibody, and then detected NP by Western Blot. We could readily co-precipitate NP with CAD, indicating that CAD is able to interact with NP (Figure 6). Because NP is an RNA-binding protein [36], we also tested whether this interaction between CAD and NP is RNA dependent by treating the samples prior to coIP with RNase A. Under these conditions, we were still able to co-precipitate NP with CAD, demonstrating that the interaction between CAD and NP is not dependent on the presence of RNA (Figure 6).

Peer-reviewed version available at Cells 2020, 9, 1126; doi:10.3390/cells9051126

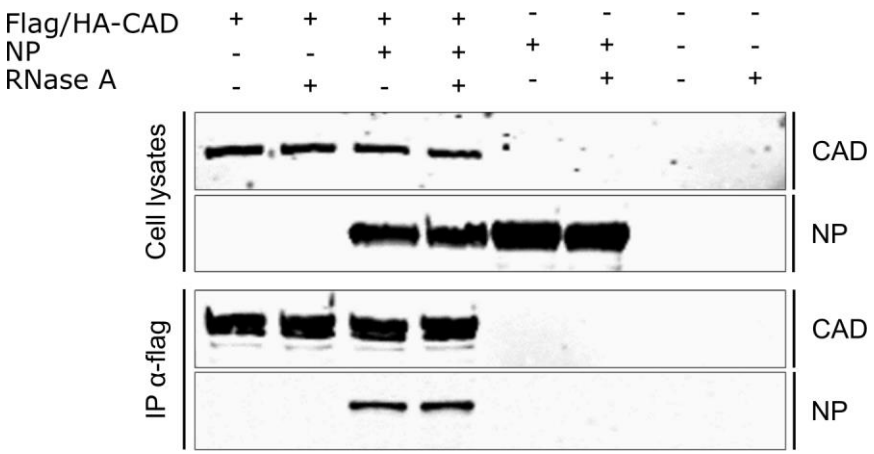

Figure 6. Interaction of CAD with NP. 293T cells were transfected with the plasmids encoding for flag/HA-CAD and EBOV-NP. 48 hours post transfection cells were lysed and treated with RNase A (100 µg/ml) or remained untreated. Flag/HA-CAD was precipitated using anti-flag antibodies, and input and precipitates were analyzed via SDS-PAGE and Western Blotting using anti-flag and anti-NP antibodies.

4. Discussion

In this work, we identified CAD, an essential component of the *de novo* pyrimidine synthesis pathway, to be important for both EBOV genome replication and transcription, and demonstrated that the function of CAD in pyrimidine synthesis is responsible for this effect. Knockdown of CAD has also been shown to affect replication and transcription of other viruses, e.g. Hepatitis C viruses [37]. Furthermore, inhibitors of CAD, e.g. the antinucleoside *N*-phosphonacetyl-L-aspartate (PALA), which transiently inhibits the aspartate transcarbamylase activity of CAD, were effective *in vitro* against various viruses including Vaccinia and arenaviruses [38,39]. The fact that this compounds exhibit antiviral activity against a broad range of viruses qualifies CAD as a promising indirect antiviral target. However, whether PALA shows antiviral efficiency against EBOV remains to be investigated.

Our results are consistent with the fact that several pyrimidine synthesis inhibitors are effective against EBOV *in vitro*, underlining the importance of the pyrimidine pathway for these viruses [20,40]. Examples are the FDA-approved drug leflunomide and its active metabolite teriflunomide, as well as SW835, a racemic version of GSK983, which has been described to exhibit a broad-spectrum antiviral activity [20,40,41]. These compounds all impair the *de novo* pyrimidine biosynthesis through inhibition of dihydroorotate dehydrogenase (DHODH), an enzyme downstream of CAD in the pyrimidine pathway. Interestingly, treatment with these inhibitors seems to have similar inhibitory effects on EBOV minigenome assays compared to the effect we observe for CAD knockdown, although CAD activity is not directly affected [20,40]. Provision of pyrimidines or upstream metabolites, e.g. orotic acid, reversed antiviral activity of all pyrimidine pathway inhibitors in EBOV minigenome assays, which is in line with our observation that supplementation with pyrimidines restores reporter activity after CAD knockdown. Interestingly, inhibition of DHODH by using SW835 not only showed pyrimidine depletion, but also stimulated ISG expression, which contributes to the activation of innate immune response [40]. However, until now the mechanism behind the stimulation of innate immune response by DHODH inhibitors remains incompletely understood and needs to be further analyzed.

We were further able to show that CAD is recruited to EBOV inclusion bodies, which represent the site of EBOV replication and transcription [8,9]. Since we observed CAD recruitment into NP-induced inclusion bodies during single expression of NP, and detected an interaction of CAD with NP using CoIP studies, we suggest that this recruitment is mediated via an interaction of CAD with NP. So far, knowledge about direct interactions between CAD and proteins of other viruses is limited, but Angeletti *et al.* showed that CAD recruits the preterminal protein (pTP) of adenoviruses to the

Peer-reviewed version available at Cells 2020, 9, 1126; doi:10.3390/cells9051126

site of adenovirus replication in the nuclear matrix via direct interaction. This interaction is believed to be required for anchorage of the adenovirus replication complex at the nuclear matrix in close proximity of required cellular factors to segregate replicated and genomic viral DNA [42,43].

In the context of its cellular function, CAD has been shown to localize primarily in the cytoplasm, although small amounts can also be detected in the nucleus of dividing cells. Redistribution of CAD in nuclear compartments during cell growth and proliferation is believed to be in response to phosphorylation by MAP kinases at position Thr-456, which results in upregulation of the enzymatic activity of CAD [30]. Since NP is known to recruit a number of factors, including kinases and phosphatases, into inclusion bodies [16-18], it is possible that recruited CAD is activated in inclusion bodies in order to provide pyrimidines for EBOV replication and transcription. However, CAD lacking the CPS domain (CAD-ΔCPS), which contains Thr-456, was still recruited into NP-induced inclusion bodies, excluding a selective recruitment of Thr-456-phosphorylated and thus activated CAD into inclusion bodies.

Overall, we have shown that CAD is recruited into NP-induced and virus-induced inclusion bodies to provide sufficient amounts of pyrimidines for EBOV genome replication and transcription. Furthermore, we demonstrated that the GLN domain of CAD is required for recruitment into inclusion bodies. These findings increase our understanding of EBOV and its host cell interactions, and provide a basis for future identification of molecular targets for the development of novel therapeutics against this virus.

Supplementary Materials: The following are available online, Figure S1: Comparisonof T7 and Pol-II-driven replication-deficient minigenomes.

Author Contributions Conceptualization: JB, LW, TH; Investigation: JB, LW, BB, TH; Supervision: TCM, TH; Visualization: JB, TH; Funding acquisition: TH; Writing – Original Draft Preparation: JB, TH.

Funding: Funding was provided by the Deutsche Forschungsgemeinschaft (DFG), grant number 389002253, (JB, LW), and by the Friedrich-Loeffler-Institut, intramural funding (TH) and funding as part of the VISION consortium (BB).

Acknowledgments: The authors would like to thank Logan Banadyga (Public Health Agency of Canada) for his help in establishing the coIP procedure, and Stephan Becker (Philipps University Marburg) for providing the Huh7 cells. We further thank Luca Zaeck (Friedrich-Loeffler-Institut) for technical assistance with the confocal microscope as well as Allison Groseth and Sandra Diederich (Friedrich-Loeffler-Institut) for technical assistance with BSL4 work.

Conflicts of Interest: The authors declare no conflict of interest. The funders had no role in the design of the study; in the collection, analyses, or interpretation of data; in the writing of the manuscript, or in the decision to publish the results.

References

1. Feldmann, H.; Geisbert, T.W. Ebola haemorrhagic fever. *Lancet* **2011**, *377*, 849-862, doi:10.1016/S0140-6736(10)60667-8.
2. Burk, R.; Bollinger, L.; Johnson, J.C.; Wada, J.; Radoshitzky, S.R.; Palacios, G.; Bavari, S.; Jahrling, P.B.; Kuhn, J.H. Neglected filoviruses. *FEMS Microbiol Rev* **2016**, *40*, 494-519, doi:10.1093/femsre/fuw010.
3. Bharat, T.A.; Noda, T.; Riches, J.D.; Kraehling, V.; Kolesnikova, L.; Becker, S.; Kawaoka, Y.; Briggs, J.A. Structural dissection of Ebola virus and its assembly determinants using cryo-electron tomography. *Proc Natl Acad Sci U S A* **2012**, *109*, 4275-4280, doi:10.1073/pnas.1120453109.
4. Ruigrok, R.W.; Crepin, T.; Kolakofsky, D. Nucleoproteins and nucleocapsids of negative-strand RNA viruses. *Curr Opin Microbiol* **2011**, *14*, 504-510, doi:10.1016/j.mib.2011.07.011.
5. Becker, S.; Rinne, C.; Hofsass, U.; Klenk, H.D.; Muhlberger, E. Interactions of Marburg virus nucleocapsid proteins. *Virology* **1998**, *249*, 406-417, doi:10.1006/viro.1998.9328.
6. Muhlberger, E.; Weik, M.; Volchkov, V.E.; Klenk, H.D.; Becker, S. Comparison of the transcription and replication strategies of marburg virus and Ebola virus by using artificial replication systems. *J Virol* **1999**, *73*, 2333-2342.

Peer-reviewed version available at Cells 2020, 9, 1126; doi:10.3390/cells9051126

7. Weik, M.; Modrof, J.; Klenk, H.D.; Becker, S.; Muhlberger, E. Ebola virus VP30-mediated transcription is regulated by RNA secondary structure formation. *J Virol* **2002**, *76*, 8532-8539, doi:10.1128/jvi.76.17.8532-8539.2002.
8. Hoenen, T.; Shabman, R.S.; Groseth, A.; Herwig, A.; Weber, M.; Schudt, G.; Dolnik, O.; Basler, C.F.; Becker, S.; Feldmann, H. Inclusion bodies are a site of ebolavirus replication. *J Virol* **2012**, *86*, 11779-11788, doi:10.1128/JVI.01525-12.
9. Lier, C.; Becker, S.; Biedenkopf, N. Dynamic phosphorylation of Ebola virus VP30 in NP-induced inclusion bodies. *Virology* **2017**, *512*, 39-47, doi:10.1016/j.virol.2017.09.006.
10. Boehmann, Y.; Enterlein, S.; Randolf, A.; Muhlberger, E. A reconstituted replication and transcription system for Ebola virus Reston and comparison with Ebola virus Zaire. *Virology* **2005**, *332*, 406-417, doi:10.1016/j.virol.2004.11.018.
11. Groseth, A.; Charton, J.E.; Sauerborn, M.; Feldmann, F.; Jones, S.M.; Hoenen, T.; Feldmann, H. The Ebola virus ribonucleoprotein complex: a novel VP30-L interaction identified. *Virus Res* **2009**, *140*, 8-14, doi:10.1016/j.virusres.2008.10.017.
12. Fang, J.; Pietzsch, C.; Ramanathan, P.; Santos, R.I.; Ilinykh, P.A.; Garcia-Blanco, M.A.; Bukreyev, A.; Bradrick, S.S. Staufen1 Interacts with Multiple Components of the Ebola Virus Ribonucleoprotein and Enhances Viral RNA Synthesis. *mBio* **2018**, *9*, doi:10.1128/mBio.01771-18.
13. Chen, J.; He, Z.; Yuan, Y.; Huang, F.; Luo, B.; Zhang, J.; Pan, T.; Zhang, H.; Zhang, J. Host factor SMYD3 is recruited by Ebola virus nucleoprotein to facilitate viral mRNA transcription. *Emerg Microbes Infect* **2019**, *8*, 1347-1360, doi:10.1080/22221751.2019.1662736.
14. Batra, J.; Hultquist, J.F.; Liu, D.; Shtanko, O.; Von Dollen, J.; Satkamp, L.; Jang, G.M.; Luthra, P.; Schwarz, T.M.; Small, G.I., et al. Protein Interaction Mapping Identifies RBBP6 as a Negative Regulator of Ebola Virus Replication. *Cell* **2018**, *175*, 1917-1930 e1913, doi:10.1016/j.cell.2018.08.044.
15. Gabriel, G.; Feldmann, F.; Reimer, R.; Thiele, S.; Fischer, M.; Hartmann, E.; Bader, M.; Ebihara, H.; Hoenen, T.; Feldmann, H. Importin-alpha7 Is Involved in the Formation of Ebola Virus Inclusion Bodies but Is Not Essential for Pathogenicity in Mice. *J Infect Dis* **2015**, *212 Suppl 2*, S316-321, doi:10.1093/infdis/jiv240.
16. Morwitzer, M.J.; Tritsch, S.R.; Cazares, L.H.; Ward, M.D.; Nuss, J.E.; Bavari, S.; Reid, S.P. Identification of RUVBL1 and RUVBL2 as Novel Cellular Interactors of the Ebola Virus Nucleoprotein. *Viruses* **2019**, *11*, doi:10.3390/v11040372.
17. Kruse, T.; Biedenkopf, N.; Hertz, E.P.T.; Dietzel, E.; Stalmann, G.; Lopez-Mendez, B.; Davey, N.E.; Nilsson, J.; Becker, S. The Ebola Virus Nucleoprotein Recruits the Host PP2A-B56 Phosphatase to Activate Transcriptional Support Activity of VP30. *Mol Cell* **2018**, *69*, 136-145 e136, doi:10.1016/j.molcel.2017.11.034.
18. Takamatsu, Y.; Krahling, V.; Kolesnikova, L.; Halwe, S.; Lier, C.; Baumeister, S.; Noda, T.; Biedenkopf, N.; Becker, S. Serine-Arginine Protein Kinase 1 Regulates Ebola Virus Transcription. *mBio* **2020**, *11*, doi:10.1128/mBio.02565-19.
19. Wendt, L.; Brandt, J.; Bodmer, B.S.; Reiche, S.; Schmidt, M.L.; Traeger, S.; Hoenen, T. The Ebola Virus Nucleoprotein Recruits the Nuclear RNA Export Factor NXF1 into Inclusion Bodies to Facilitate Viral Protein Expression. *Cells* **2020**, *9*, doi:10.3390/cells9010187.
20. Martin, S.; Chiramel, A.I.; Schmidt, M.L.; Chen, Y.C.; Whitt, N.; Watt, A.; Dunham, E.C.; Shifflett, K.; Traeger, S.; Leske, A., et al. A genome-wide siRNA screen identifies a druggable host pathway essential for the Ebola virus life cycle. *Genome Med* **2018**, *10*, 58, doi:10.1186/s13073-018-0570-1.
21. Uebelhoer, L.S.; Albarino, C.G.; McMullan, L.K.; Chakrabarti, A.K.; Vincent, J.P.; Nichol, S.T.; Towner, J.S. High-throughput, luciferase-based reverse genetics systems for identifying inhibitors of Marburg and Ebola viruses. *Antiviral Res* **2014**, *106*, 86-94, doi:10.1016/j.antiviral.2014.03.018.
22. Nelson, E.V.; Pacheco, J.R.; Hume, A.J.; Cressey, T.N.; Deflube, L.R.; Ruedas, J.B.; Connor, J.H.; Ebihara, H.; Muhlberger, E. An RNA polymerase II-driven Ebola virus minigenome system as an advanced tool for antiviral drug screening. *Antiviral Res* **2017**, *146*, 21-27, doi:10.1016/j.antiviral.2017.08.005.
23. Coleman, P.F.; Suttle, D.P.; Stark, G.R. Purification from hamster cells of the multifunctional protein that initiates de novo synthesis of pyrimidine nucleotides. *J Biol Chem* **1977**, *252*, 6379-6385.
24. Jones, M.E. Pyrimidine nucleotide biosynthesis in animals: genes, enzymes, and regulation of UMP biosynthesis. *Annu Rev Biochem* **1980**, *49*, 253-279, doi:10.1146/annurev.bi.49.070180.001345.
25. Lee, L.; Kelly, R.E.; Pastra-Landis, S.C.; Evans, D.R. Oligomeric structure of the multifunctional protein CAD that initiates pyrimidine biosynthesis in mammalian cells. *Proc Natl Acad Sci U S A* **1985**, *82*, 6802-6806, doi:10.1073/pnas.82.20.6802.

Peer-reviewed version available at Cells 2020, 9, 1126; doi:10.3390/cells9051126

26. Christopherson, R.I.; Jones, M.E. The overall synthesis of L-5,6-dihydroorotate by multienzymatic protein pyr1-3 from hamster cells. Kinetic studies, substrate channeling, and the effects of inhibitors. *J Biol Chem* **1980**, *255*, 11381-11395.
27. Irvine, H.S.; Shaw, S.M.; Paton, A.; Carrey, E.A. A reciprocal allosteric mechanism for efficient transfer of labile intermediates between active sites in CAD, the mammalian pyrimidine-biosynthetic multienzyme polypeptide. *Eur J Biochem* **1997**, *247*, 1063-1073, doi:10.1111/j.1432-1033.1997.01063.x.
28. Evans, D.R.; Guy, H.I. Mammalian pyrimidine biosynthesis: fresh insights into an ancient pathway. *J Biol Chem* **2004**, *279*, 33035-33038, doi:10.1074/jbc.R400007200.
29. Sigoillot, F.D.; Berkowski, J.A.; Sigoillot, S.M.; Kotsis, D.H.; Guy, H.I. Cell cycle-dependent regulation of pyrimidine biosynthesis. *J Biol Chem* **2003**, *278*, 3403-3409, doi:10.1074/jbc.M211078200.
30. Sigoillot, F.D.; Kotsis, D.H.; Serre, V.; Sigoillot, S.M.; Evans, D.R.; Guy, H.I. Nuclear localization and mitogen-activated protein kinase phosphorylation of the multifunctional protein CAD. *J Biol Chem* **2005**, *280*, 25611-25620, doi:10.1074/jbc.M504581200.
31. Chaparian, M.G.; Evans, D.R. Intracellular location of the multidomain protein CAD in mammalian cells. *FASEB J* **1988**, *2*, 2982-2989, doi:10.1096/fasebj.2.14.2903106.
32. Hoenen, T.; Jung, S.; Herwig, A.; Groseth, A.; Becker, S. Both matrix proteins of Ebola virus contribute to the regulation of viral genome replication and transcription. *Virology* **2010**, *403*, 56-66, doi:10.1016/j.virol.2010.04.002.
33. Shabman, R.S.; Hoenen, T.; Groseth, A.; Jabado, O.; Binning, J.M.; Amarasinghe, G.K.; Feldmann, H.; Basler, C.F. An upstream open reading frame modulates ebola virus polymerase translation and virus replication. *PLoS Pathog* **2013**, *9*, e1003147, doi:10.1371/journal.ppat.1003147.
34. Kamper, L.; Zierke, L.; Schmidt, M.L.; Muller, A.; Wendt, L.; Brandt, J.; Hartmann, E.; Braun, S.; Holzerland, J.; Groseth, A., et al. Assessment of the function and intergenus-compatibility of Ebola and Lloviu virus proteins. *J Gen Virol* **2019**, *100*, 760-772, doi:10.1099/jgv.0.001261.
35. Huang, Y.; Xu, L.; Sun, Y.; Nabel, G.J. The assembly of Ebola virus nucleocapsid requires virion-associated proteins 35 and 24 and posttranslational modification of nucleoprotein. *Mol Cell* **2002**, *10*, 307-316, doi:10.1016/s1097-2765(02)00588-9.
36. Noda, T.; Hagiwara, K.; Sagara, H.; Kawaoka, Y. Characterization of the Ebola virus nucleoprotein-RNA complex. *J Gen Virol* **2010**, *91*, 1478-1483, doi:10.1099/vir.0.019794-0.
37. Borawski, J.; Troke, P.; Puyang, X.; Gibaja, V.; Zhao, S.; Mickanin, C.; Leighton-Davies, J.; Wilson, C.J.; Myer, V.; Cornellataracido, I., et al. Class III phosphatidylinositol 4-kinase alpha and beta are novel host factor regulators of hepatitis C virus replication. *J Virol* **2009**, *83*, 10058-10074, doi:10.1128/JVI.02418-08.
38. Ortiz-Riano, E.; Ngo, N.; Devito, S.; Eggink, D.; Munger, J.; Shaw, M.L.; de la Torre, J.C.; Martinez-Sobrido, L. Inhibition of arenavirus by A3, a pyrimidine biosynthesis inhibitor. *J Virol* **2014**, *88*, 878-889, doi:10.1128/JVI.02275-13.
39. Katsafanas, G.C.; Grem, J.L.; Blough, H.A.; Moss, B. Inhibition of vaccinia virus replication by N-(phosphonoacetyl)-L-aspartate: differential effects on viral gene expression result from a reduced pyrimidine nucleotide pool. *Virology* **1997**, *236*, 177-187, doi:10.1006/viro.1997.8735.
40. Luthra, P.; Naidoo, J.; Pietzsch, C.A.; De, S.; Khadka, S.; Anantpadma, M.; Williams, C.G.; Edwards, M.R.; Davey, R.A.; Bukreyev, A., et al. Inhibiting pyrimidine biosynthesis impairs Ebola virus replication through depletion of nucleoside pools and activation of innate immune responses. *Antiviral Res* **2018**, *158*, 288-302, doi:10.1016/j.antiviral.2018.08.012.
41. Deans, R.M.; Morgens, D.W.; Okesli, A.; Pillay, S.; Horlbeck, M.A.; Kampmann, M.; Gilbert, L.A.; Li, A.; Mateo, R.; Smith, M., et al. Parallel shRNA and CRISPR-Cas9 screens enable antiviral drug target identification. *Nat Chem Biol* **2016**, *12*, 361-366, doi:10.1038/nchembio.2050.
42. Angeletti, P.C.; Engler, J.A. Adenovirus preterminal protein binds to the CAD enzyme at active sites of viral DNA replication on the nuclear matrix. *J Virol* **1998**, *72*, 2896-2904.
43. Fredman, J.N.; Engler, J.A. Adenovirus precursor to terminal protein interacts with the nuclear matrix in vivo and in vitro. *J Virol* **1993**, *67*, 3384-3395.